# High-spin states in the nuclei $^{91}$Y and $^{95}$Nb

D. Bucurescu,[1] Zs. Podolyák,[2] C. Rusu,[1,3] G. de Angelis,[3] Y. H. Zhang,[3] G. Căta-Danil,[1] I. Căta-Danil,[1] M. Ivaşcu,[1] N. Mărginean,[1,3] R. Mărginean,[1] L. C. Mihăilescu,[1] G. A. Suliman,[1] P. H. Regan,[2] W. Gelletly,[2] S. D. Langdown,[2] J. J. Valiente Dobón,[2] D. Bazzacco,[4] S. Lunardi,[4] C. A. Ur,[4] M. Axiotis,[3] A. Gadea,[3] E. Farnea,[3] M. Ionescu-Bujor,[1] A. Iordăchescu,[1] Th. Kröll,[3] T. Martinez,[3] P. G. Bizzetti,[5] R. Broda,[6] N. H. Medina,[7] B. Quintana,[8] and B. Rubio[9]

[1]*H. Hulubei National Institute for Physics and Nuclear Engineering, Bucharest, Romania*
[2]*Department of Physics, University of Surrey, Guildford, GU2 7XH, UK*
[3]*Istituto Nazionale di Física Nucleare (INFN), Laboratori Nazionali di Legnaro, Italy*
[4]*Dipartimento di Fisica dell'Università and INFN, Sezione di Padova, Italy*
[5]*Dipartimento di Fisica and INFN, Firenze, Italy*
[6]*Niewodniczanski Institute of Nuclear Physics, Krakow, Poland*
[7]*Instituto de Física, Universidade de Šao Paulo, Šao Paulo, Brazil*
[8]*Grupo de Física Nuclear, Universidad de Salamanca, Spain*
[9]*Instituto de Física Corpuscular, València, Spain*

(Received 26 July 2004; published 22 March 2005)

The positive-parity yrast states in the $^{91}$Y and $^{95}$Nb nuclei have been studied by $\gamma$-ray spectroscopy following heavy-ion-induced fusion-evaporation reactions. The lowest-lying transitions in these structures have been assigned via the $p2n$ channel of the reactions of $^{12}$C (38 MeV) and $^{16}$O (48 MeV) beams with a $^{82}$Se target, studied at the Bucharest Tandem accelerator. More detailed level schemes have been determined subsequently in a study performed with the GASP array of the inverse reactions produced by a $^{82}$Se (470 MeV) beam from the Legnaro Tandem-LINAC accelerator with oxygen and possibly carbon contaminants of a $^{192}$Os target. The observed level schemes are compared with local systematics and shell-model calculations.

DOI: 10.1103/PhysRevC.71.034315 PACS number(s): 23.20.Lv, 21.60.Cs, 25.70.Jj, 27.60.+j

## I. INTRODUCTION

Nuclei in the $A \approx 100$ region with neutron number above 50 generally follow a transition from spherical toward prolate deformed ground states. Particularly interesting in this region is the onset of large nuclear deformation which takes place between $N = 58$ and $N = 60$ and is rather sudden in the Sr and Zr isotopes and more gradual in the Mo isotopes. For the nuclei closer to $N = 50$, the structure is generally understood in terms of simple excitations across the subshell closures at 50 and 56.

There are, however, some nuclei in this region which are rather poorly known at higher spins. The nuclei studied in this work, $^{91}$Y and $^{95}$Nb, are two such examples. This situation occurs because they are rather close to the stability line and therefore are not so readily populated in reactions that bring in significant angular momentum, such as the fusion-evaporation reaction. Consequently, for such studies one needs $\gamma$-ray coincidence setups with high efficiency.

The $^{91}$Y nucleus has been studied before only in $\beta$ decay [1] and light-particle-induced transfer reactions: $(t, p)$ [2], $(d, ^3\mathrm{He})$ and $(t, \alpha)$ [3], and $(p, \alpha)$ [4]. Thus, only relatively low-spin states are known in this nucleus (see the adopted level scheme in Ref. [5]). Similarly, the structure of $^{95}$Nb is known only from studies of $\beta$ decay [6] and reactions with light projectiles: $(p, p')$ [7], $(^3\mathrm{He}, d)$, and $(\alpha, t)$ [8]; $(t, \alpha)$ [9], and $(d, \alpha)$ [10] (see also the adopted level scheme in Ref. [11]).

In the present work, we show new results on the high-spin states of the $^{91}\mathrm{Y}_{52}$ and $^{95}\mathrm{Nb}_{54}$ nuclei, thus enriching the systematics of the nuclear structure evolution along the $N = 52$ and $N = 54$ chains. A comparison between the experimental results and shell-model calculations will be made for both nuclei.

## II. EXPERIMENTAL

### A. Experiments with $^{12}$C and $^{16}$O beams

High-spin states in the $^{91}$Y and $^{95}$Nb nuclei have been populated in fusion-evaporation reactions. The first series of experiments were performed at the Bucharest FN tandem accelerator. The beams were $^{12}$C at 38 MeV and $^{16}$O at 48 MeV, with currents typically around 10 particle nA. The target was in both cases a $\sim$3-mg/cm$^2$ selenium (enriched 92% in $^{82}$Se), vacuum evaporated onto a 2-mg/cm$^2$ Au foil.

The $\gamma$ rays were detected with three $\sim$20% efficiency HPGe detectors, placed at 45°, 135°, and 270° with respect to the beam direction, and one planar Ge detector placed in the same plane at 215°. The charged particles from the reaction were detected with a $\Delta E$-$E$ telescope with silicon detectors of thicknesses of 0.15 and 0.5 mm and an active surface of 150 mm$^2$. The telescope was mounted at 60° in the forward direction, at a distance of 2.5 cm from the target, and was screened against the scattered heavy ions with a 70-$\mu$m-thick Al foil. Neutrons were detected with a 1 litre NE213 scintillator detector placed in the forward direction, shielded with 2.5 cm of lead and covering $\pm 28°$; the neutron-$\gamma$ discrimination was made by pulse-shape analysis. Coincidences between all these detectors were registered on the hard disk of a PC and then analyzed off-line by generating $\gamma$-ray spectra coincident with neutrons, protons, and $\alpha$ particles, as well as $\gamma$-$\gamma$ coincidence

 ©2005 The American Physical Society

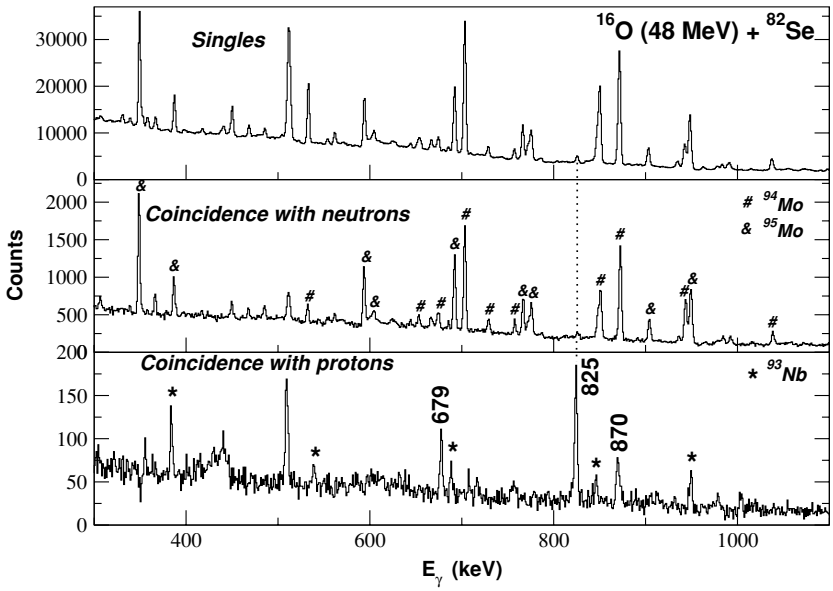


FIG. 1. $\gamma$-ray spectra measured in the reaction $^{82}$Se + $^{16}$O (48 MeV). The singles and neutron-coincident spectra are dominated by transitions (marked) of the dominant channels $4n$ ($^{84}$Mo) and $3n$ ($^{85}$Mo) [16]. The transitions labeled with their energies in the bottom spectrum have been assigned to $^{95}$Nb.

matrices. About $5\times10^7$ events were registered in each of these experiments. $\gamma$-ray energy and efficiency calibrations were made with a $^{152}$Eu source.

These experiments had as their main purpose the assignment of new $\gamma$-ray transitions to the positive-parity yrast lines of the two nuclei (see below).

### B. Experiment with $^{82}$Se beam

The lowest-lying few transitions in the yrast bands of $^{91}$Y and $^{95}$Nb, as determined from the experiments described above, were used as starting points to extend the level scheme by working on data from an experiment performed with the GASP array. This was a multinucleon transfer reaction experiment made with a $^{82}$Se beam on a $^{192}$Os target, aimed at obtaining new information on the level schemes of W and Os targetlike nuclei and Ge beamlike nuclei [12]. The $^{82}$Se beam had an energy of 470 MeV and current of about 1 particle nA and was accelerated by the XTU Tandem and ALPI Linac accelerators from Legnaro. The target was 50 mg/cm$^2$ thick, on a 0.2-mm Ta foil. The nuclei of interest for the present work were populated in the fusion-evaporation reactions of the Se beam with $^{16}$O and, possibly, $^{12}$C contaminants of the target. Calculations with the statistical model code CASCADE show that at 470-MeV energy of the $^{82}$Se beam, and lower energies due to its fast slowing down in the Os target, the reactions on $^{16}$O appreciably populate a wide range of nuclei: $^{94}$Mo($4n$ channel), $^{95-92}$Nb ($pxn$), $^{93-90}$Zr ($\alpha xn$), $^{91-89}$Y ($\alpha pxn$). The observed relative intensities of the different channels are difficult to compare more than qualitatively with the calculations, because of the unknown distribution of oxygen in the target, but they suggest an in-depth oxidization of the target: the comparable intensities observed for $^{95}$Nb

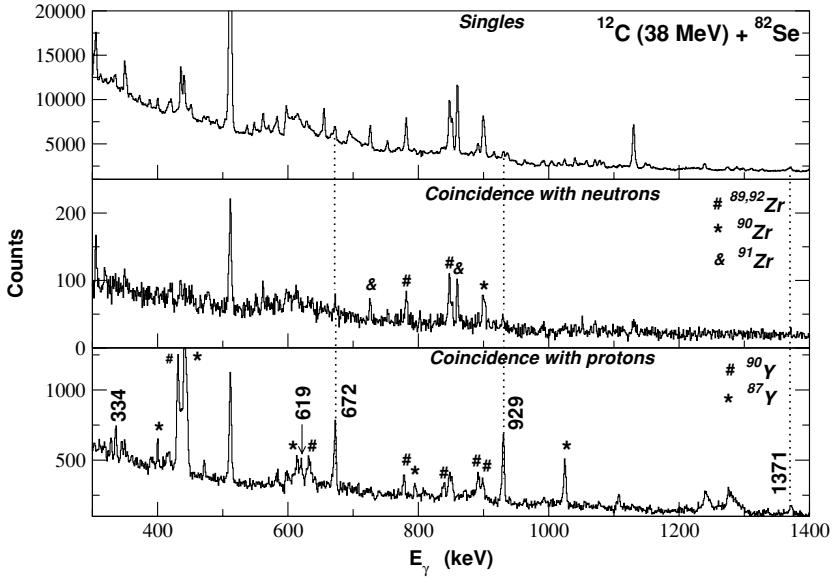


FIG. 2. Similar to Fig. 1, but for the $^{82}$Se + $^{12}$C (38 MeV) reaction. The transitions labeled with their energies in the bottom spectrum have been assigned to $^{91}$Y.

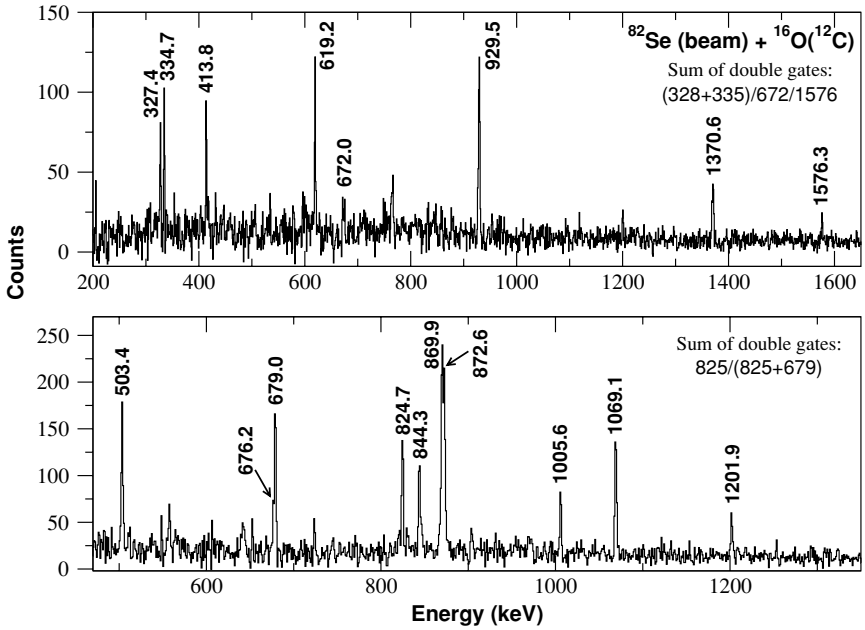


FIG. 3. Examples of triple $\gamma$-ray coincidences illustrating the level schemes presented in Figs. 4 (upper spectrum) and 5 (lower spectrum). The displayed spectra were obtained in the reactions of the $^{82}$Se beam with oxygen, and possibly with carbon contaminants of the Os target, by double gating on a symmetric cube; they are a sum of the coincidences between any two $\gamma$-ray transitions specified in the shown groups.

(the $p2n$ channel) and $^{91}$Y ($\alpha p2n$) could be explained by their cross sections integrated over the range 470 to about 200 MeV (reached by the incident beam after traveling $\sim$15 mg/cm$^2$ in the target). On the other hand, some contribution to the $^{91}$Y production may come also from the reaction of the $^{82}$Se beam with a $^{12}$C contaminant, as shown by the production of some Sr isotopes ($\alpha xn$ channels), but it is expected that this contribution is less important than that of the reaction on oxygen, since the carbon impurity can only be imagined as being due to a thin layer of, e.g., vacuum oil, at the surface of the target.

In this experiment, the $\gamma$ rays were detected with the GASP array [13] in a configuration with 40 HPGe detectors and 74 BGO detectors as a multiplicity filter (6 of the 80 BGO elements of GASP were replaced by neutron detectors at the time of the experiment). The events registered on tape had as their trigger the condition that at least three Ge detectors and two BGO's were in coincidence. In the off-line processing of the data, two- and three-dimensional symmetrized $\gamma$-coincident matrices were constructed, as well as different nonsymmetric matrices. Thus, in order to obtain angular distribution (ADO) information, $\gamma$-$\gamma$ matrices were made, in which the energy signals from all detectors were registered on one axis, and those from each specific ring of detectors were put on the other axis. By gating on the all-detector axis, the resulting spectra have the ADO information independent of the gating transition(s). Another type of nonsymmetric $\gamma$-$\gamma$ matrix was also made, with the 90° detector ring on one axis, and the 34° and 146° rings on the other axis; this matrix was used to determine directional correlation orientation (DCO) ratios for the assignment of multipolarities to the $\gamma$-ray transitions.

## III. RESULTS

Figures 1 and 2 illustrate the results obtained in the experiments with the light-ion beams. Figure 1 shows $\gamma$-ray spectra from the $^{82}$Se + $^{16}$O (48 MeV) reaction, recorded in the singles mode as well as in coincidence with neutrons and protons. The spectrum in coincidence with protons shows, besides weak lines of $^{93}$Nb [14] (from the target contamination with $^{80}$Se), three unknown $\gamma$ rays at 824.7, 679.0, and 869.9 keV. These

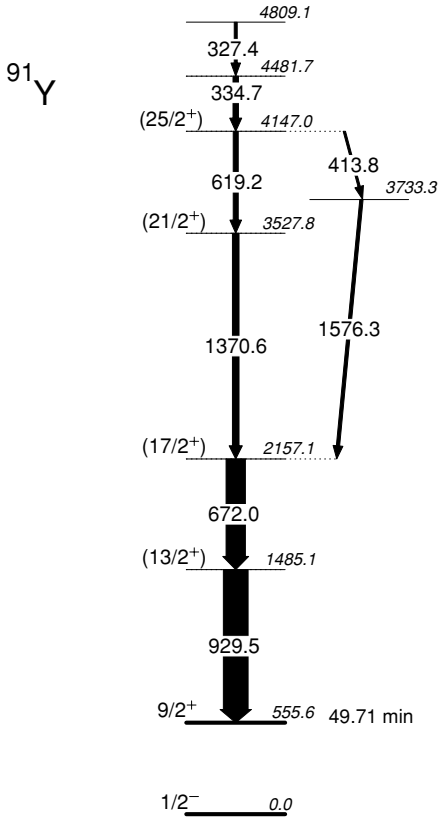


FIG. 4. Positive-parity yrast level scheme $^{91}$Y as determined from the present experiments.

lines are not seen in coincidence with $\alpha$ particles. They cannot belong to a channel with three evaporated protons—statistical model calculations with the CASCADE code predict negligible cross sections for such channels. Other channels with two evaporated protons are also predicted with very small cross sections, and in fact, none of the known $\gamma$ rays of $^{95}$Zr [15] (the $2pn$ channel) have been observed. The 824.7 keV line is also clearly seen in coincidence with the neutrons; the other two lines in the neutron-coincident spectrum are difficult to distinguish due to their proximity to lines of close energy from the much stronger, dominating channels $4n$ ($^{94}$Mo) and $3n$ ($^{95}$Mo) [16]. For the strongest $\gamma$ ray of 824.7 keV, the neutron multiplicity of the channel has been determined from the ratio of its intensity in coincidence with the neutrons and in the singles spectrum (normalized with channels with known neutron multiplicity) as $2.1 \pm 0.9$. Although it has a large statistical error caused by the low cross section of the channel, this value indicates as very likely a channel with two evaporated neutrons. Considering all the possibilities discussed above, we have finally assigned these $\gamma$ rays to the $p2n$ channel ($^{95}$Nb). The cross section of this channel, estimated relative to that of the strong $xn$ channels such as $^{94}$Mo and $^{95}$Mo [16] which are well predicted by the CASCADE calculations, is about 5 mb (ca. 2.5% of the total fusion cross section). Gating on the symmetric $\gamma$-$\gamma$ matrix revealed that the 824.7-keV transition is coincident with itself and therefore is a doublet, and that the four $\gamma$ rays form a cascade. Since it is the strongest sequence populated in the fusion-evaporation reaction, this cascade of four transitions has been assigned to the positive-parity yrast band built on the $9/2^+$ ground state of $^{95}$Nb. The small cross section of this channel combined with the reduced $\gamma$-ray detection efficiency of our setup (in the oxygen-beam experiment) did not allow a clear assignment of other transitions. Because of the weak statistical level, the multipolarity of these $\gamma$ rays could not be assigned but was tentatively proposed on the basis of the systematic of this $g_{9/2}$ structure in the region (see below).

In a similar way, we have assigned a cascade of three transitions to $^{91}$Y, namely 929.5, 672.0, and 1370.6 keV, from the study of the reaction $^{82}$Se + $^{12}$C (38 MeV). Figure 2 shows the singles, neutron-coincident, and proton-coincident spectra for this reaction, similar to those in Fig. 1. This cascade has been assigned to the positive-parity quadrupole sequence built above the known $9/2^+$ isomer (half-life 49.7 min) at $E_x = 555.6$ keV [5]. This structure was populated with an intensity of less than 3% of the total fusion cross section.

The cascades assigned to the two nuclei have been confirmed, and the level schemes have been further extended by analysis of the data collected in the GASP experiment ($^{82}$Se beam, on the oxygen and, possibly, carbon contaminants of the $^{192}$Os target). The level schemes have been constructed on the basis of the observed coincidence and intensity relationships of the $\gamma$-ray transitions. Most of the coincidences have been observed clearly by double-gating on the symmetric $\gamma$-$\gamma$-$\gamma$ cube.

Figure 3 shows some examples of the observed coincidences in the two reactions, which illustrate the level schemes

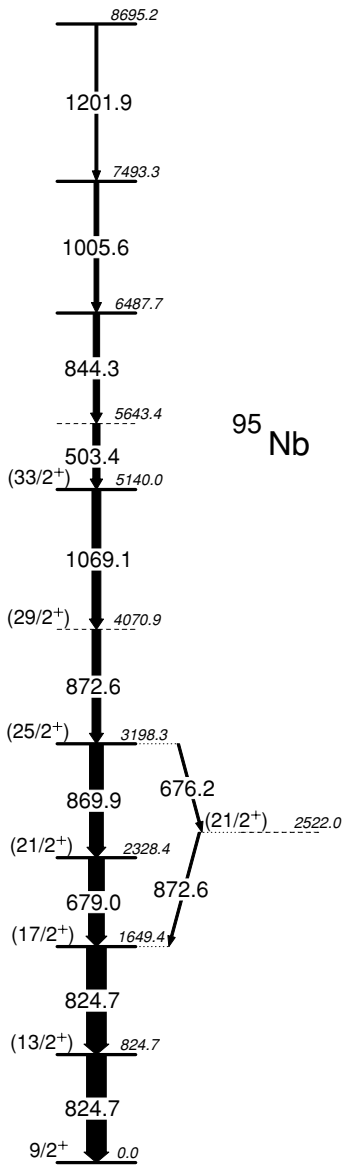


FIG. 5. Positive-parity yrast sequence of $^{95}$Nb as determined from the present experiments. The dashed lines for the levels at 2522, 4071, and 5643 keV indicate uncertainty in the ordering of the pairs of $\gamma$ rays 872.6-676.2, 872.6-1069.1, and 503.4-844.3 keV, respectively (see the intensities quoted in Table I and the discussion in the text).

deduced from the present experiments for $^{91}$Y (Fig. 4) and $^{95}$Nb (Fig. 5), respectively. Table I summarizes the information on the $\gamma$-ray transitions assigned to the two nuclei. Transition multipolarities and tentative spin-parity proposals for the levels have been made on the basis of DCO ratio, as well as ADO ratio values. DCO ratio values have been determined from the asymmetric $\gamma$-$\gamma$ coincidence matrix, by gating on transitions of known multipolarity and making the ratio

$$R_{\mathrm{DCO}} = \frac{I_{\gamma_1}(\theta_1;\ \text{gated by } \gamma_2 \text{ at } \theta_2)}{I_{\gamma_1}(\theta_2;\ \text{gated by } \gamma_2 \text{ at } \theta_1)},$$

TABLE I. $\gamma$ rays in $^{91}$Y (from the $^{12}$C+$^{82}$Se reaction) and in $^{95}$Nb (from the $^{16}$O+$^{82}$Se reaction). The relative intensities are determined from $\gamma$-gated coincidence spectra in the selenium beam (GASP) experiment; for the two lowest transitions, they were taken from the experiments with light beams. For the double $\gamma$ ray 824.7 keV in $^{95}$Nb, the assigned intensity of 100 was arbitrarily split into 50% and 50%.

| $E_\gamma$ (keV) | $E_i$ (keV) | $E_f$ (keV) | $J_i^\pi$ | $J_f^\pi$ | $I_\gamma$ | $R_{DCO}$ | $R_{ADO}$[a] |
|---|---|---|---|---|---|---|---|
| | | | $^{91}$Y | | | | |
| 327.4(2) | 4809.1 | 4481.7 | | | 11.7(15) | 1.52(61)[b] | 1.34(22) |
| 334.7(2) | 4481.7 | 4147.0 | | | 21.5(20) | 1.16(32)[b] | 1.53(20) |
| 413.8(2) | 4147.0 | 3733.3 | | | <11 | | |
| 619.2(3) | 4147.0 | 3527.8 | $(25/2^+)$ | $(21/2^+)$ | 20.2(14) | 0.85(20)[b] | 1.66(30) |
| 672.0(2) | 2157.1 | 1485.1 | $(17/2^+)$ | $(13/2^+)$ | 78(4) | 1.26(17)[c] | 1.78(12) |
| 929.5(2) | 1485.1 | 555.6 | $(13/2^+)$ | $9/2^+$ | 100(5) | | 1.37(11) |
| 1370.6(3) | 3527.8 | 2157.1 | $(21/2^+)$ | $(17/2^+)$ | 26.5(35) | 0.80(16)[b] | 1.33(20) |
| 1576.3(4) | 3733.3 | 2157.1 | - | $(17/2^+)$ | 13.2(22) | | |
| | | | $^{95}$Nb | | | | |
| 503.4(2) | 5643.4 | 5140.9 | | $(33/2^+)$ | 18.2(26) | 0.97(17)[d] | 0.96(28) |
| 676.2(3) | 3198.3 | 2522.0 | $(25/2^+)$ | $(21/2^{+}{}_2)$ | 6.0(26) | | |
| 679.0(2) | 2328.4 | 1649.4 | $(21/2^{+}{}_1)$ | $(17/2^+)$ | 40(4) | 1.13(18)[e] | 1.03(18) |
| 824.7(2)[f] | 824.7 | 0.0 | $(13/2^+)$ | $9/2^+$ | [50(6)] | | 1.18(8) |
| | 1649.4 | 824.7 | $(17/2^+)$ | $(13/2^+)$ | [50(6)] | | |
| 844.3(3) | 6487.7 | 5643.4 | | | 16.3(32) | | 1.31(24) |
| 869.9(2) | 3198.3 | 2328.4 | $(25/2^+)$ | $(21/2^{+}{}_1)$ | 35(4) | 1.22(29)[e] | 1.33(12) |
| 872.6(3)[f] | 4070.9 | 3198.3 | $(33/2^+)$ | $(29/2^+)$ | 22.3(32) | 1.07(13)[e] | |
| | 2522.0 | 1649.4 | $(21/2^{+}{}_2)$ | $(17/2^+)$ | [~6] | | |
| 1005.6(3) | 7493.3 | 6487.7 | | | 12.1(24) | 1.06(35)[d] | 1.03(17) |
| 1069.1(2) | 5140.0 | 4070.9 | $(29/2^+)$ | $(25/2^+)$ | 22.6(31) | 1.14(19)[d] | 1.26(15) |
| 1201.9(2) | 8695.2 | 7493.3 | | | 7.4(17) | | |

[a]ADO ratios determined from spectra gated by the following transitions: 929 + 672 keV in $^{91}$Y, 825 keV in $^{95}$Nb.
[b]Gate (929 + 672) keV.
[c]Gate 929 keV.
[d]Gate (825 + 679 + 870 + 872) keV.
[e]Gate 825 keV.
[f]Doubly placed $\gamma$ ray.

where $\theta_1$ and $\theta_2$ correspond to 90° and 34° or 146°, respectively. In our case the DCO ratio obtained from a gate on a stretched $\Delta J = 2$ transition should be ~1.0 for a stretched quadrupole transition and ~0.5 for a stretched $\Delta J = 1$ transition.

Alternatively, ADO ratios, defined as the ratio of the intensities of a transition as observed in the rings of detectors at 34° + 146° and at 90°, have been determined; the expected values are ~1.3 for pure quadrupole transitions and ~0.7 for pure dipole transitions.

Table I gives the values determined for both the ADO and the DCO ratios. The lowest transitions in the cascades of the two nuclei have been assigned as stretched quadrupoles, on the basis of their ADO ratio (Table I). It was assumed that they are of the $E2$ type, which also fits in the level scheme systematics of isotonic sequences (see below). DCO ratios could then be determined starting from gates on these transitions. Figure 6 shows the DCO ratio values determined for the transitions assigned to the two nuclei, in comparison with values determined for known quadrupole- and dipole-type transitions from other nuclei strongly populated in our reactions. It can be seen that the most probable assignment for our transitions is the quadrupole type. Thus, the tentative spin-parity assignments shown in Figs. 4 and 5 were made on the basis of the DCO and ADO ratios, by assuming that the quadrupole transitions are of the $E2$ type.

A special discussion is necessary in the case of $^{95}$Nb, in connection with the ordering of some of the transitions within the cascade. The 824.7-keV transition was placed as the lowest in the cascade because of the large intensity observed for this line. On the other hand, as remarked above, there is a second $\gamma$ ray with the same energy somewhere in the cascade. The place of this transition relative to the others has been deduced as follows. In a double gate on the $\gamma$-$\gamma$-$\gamma$ coincidence cube, on the 869.9- and 1069.1-keV lines, the 824.7-keV line has an intensity twice that of the 679-keV line; therefore, the three transitions of 824.7, 824.7, and 679.0 keV must be placed below the 869.9-keV transition. The 679.0-keV transition cannot be placed in between the two 824.7-keV transitions because of the observed 676.2-872.6-keV coincidence, which is an alternative path to the 869.9-679.0-keV sequence. Consequently, the lowest four transitions in the cascade are proposed in the order 824.7, 824.7, 679.0, and 869.9 keV; the intensities of the latter two transitions are determined with somewhat large

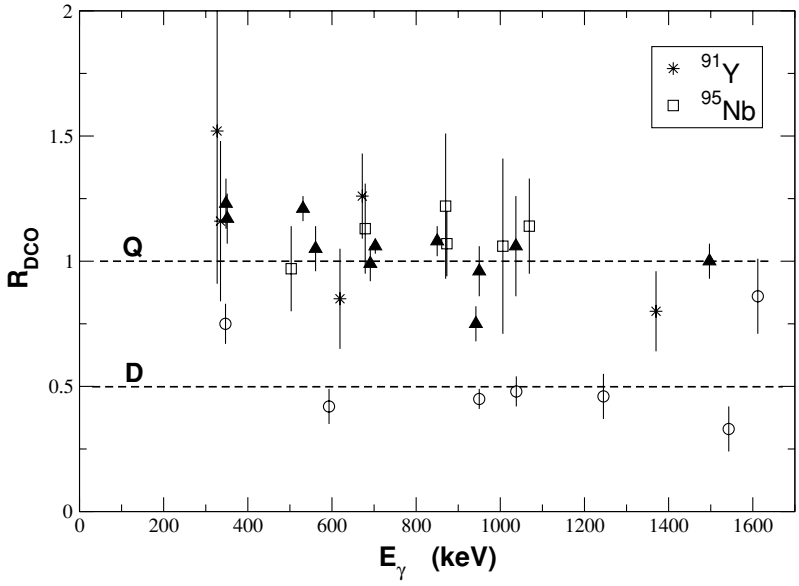


FIG. 6. DCO ratios for the transitions assigned to transitions in $^{91}$Y (stars) and $^{95}$Nb (rectangles) (Figs. 4 and 5 and Table I), compared to those of transitions of known quadrupole (Q, triangles) or dipole (D, circles) multipolarity in nuclei populated by other channels. These values have been determined by gating on quadrupole transitions.

errors (Table I), but in both experiments the intensity of the 679-keV transition is found indeed to be systematically larger than that of the 870-keV one. Above the 3198-keV level, there are two cases of uncertain ordering of pairs of $\gamma$ rays, namely, 872.6 and 1069.1 keV, and 503.4 and 844.3 keV; in both cases the two $\gamma$ rays have equal intensities within the statistical uncertainty (Table I). This is indicated in Fig. 5 by drawing the intermediate level by a dashed line. One should note, therefore, that while the positions of the levels at 5140.0 and 6487.7 keV are unambiguously determined, those of the levels at 4070.9 and 5643.4 keV could have resulted by swapping the positions of the two $\gamma$ rays that feed and deexcite these levels.

## IV. DISCUSSION

### A. Level systematics

Figure 7 shows the evolution of the lowest part of the assumed $g_{9/2}$ structure observed in $^{91}_{39}$Y in comparison with that of other odd-A $N = 52$ nuclei and the ground-state quasiband of the even-even $N = 52$ nuclei. The structure assigned to $^{91}$Y is rather similar to that of the neighboring even-even isotone $^{92}$Zr and, up to the $4^+$ state, to that of $^{90}$Sr (where the $6^+_1$ state is higher, at 1839 keV above the $4^+_1$ state). Thus, this structure can be interpreted as a $g_{9/2}$ proton hole weakly coupled to the $0^+$, $2^+$, $4^+$, and $6^+$ states of the even-even $^{92}$Zr core.

Similarly, Fig. 8 shows the evolution of the same structure along the $N = 54$ chain. This systematic shows that the first two yrast transitions of $^{95}$Nb follow smoothly the trend given by the closest $N = 54$ neighbors ($^{96}$Mo, $^{97}$Tc).

### B. Comparison with shell-model calculations

To understand the observed structure, spherical shell-model calculations have been performed with the code OXBASH [17]. We used the "gwb" model space and the residual interaction named "gwbxg" in the code. The "gwb" model space includes four valence proton orbitals ($1f_{5/2}$, $2p_{3/2}$, $2p_{1/2}$,

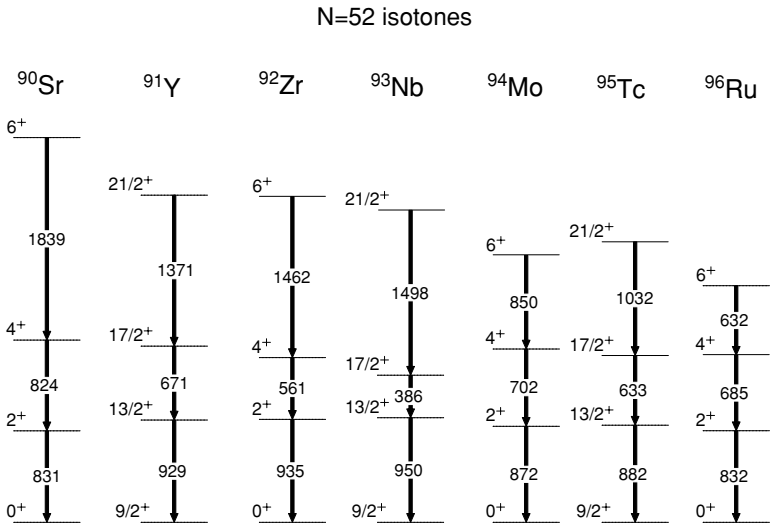


FIG. 7. Systematic of levels along the $N = 52$ isotones.

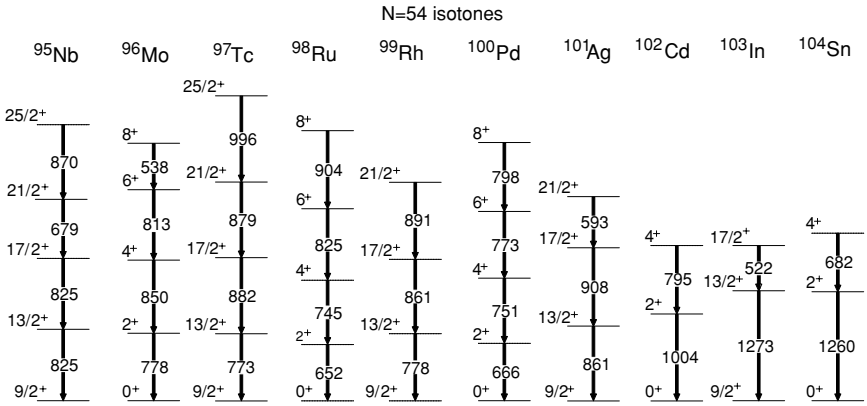


FIG. 8. Systematic of levels along the $N = 54$ isotones.

and $1g_{9/2}$) and six valence neutron orbitals ($1g_{9/2}$, $2p_{1/2}$, $2d_{5/2}$, $1g_{7/2}$, $3s_{1/2}$, and $2d_{3/2}$). The residual interaction contains a combination of calculated and empirical two-body matrix elements (TBME) which is described in the code. The original TBME are based on the bare G-matrix calculations of Ref. [18]. The TBME for the proton orbitals are replaced by the effective values of Ji and Wildenthal [19]. The TBME which connect the proton $2p_{1/2}$, $1g_{9/2}$ orbitals with the neutron $2d_{5/2}$, $3s_{1/2}$ orbitals are replaced with those determined by Gloeckner [20], and those between the proton $2p_{1/2}$, $1g_{9/2}$ orbitals with the neutron $2p_{1/2}$, $1g_{9/2}$ orbitals are replaced with those of Serduke *et al.* [21]. In our calculations for $^{95}$Nb, we assumed that $^{88}_{38}$Sr$^{50}$ is an inert core, so that the proton $1f_{5/2}$ and $2p_{3/2}$ orbitals and the neutron $1g_{9/2}$ and $2p_{1/2}$ orbitals were kept fully occupied, while in the case of $^{91}$Y we relaxed this condition for the proton orbitals allowing 1p-1h and 2p-2h excitations across the $Z = 38$ shell closure. The single-particle energies corresponding to our valence space were 0.82, 2.20, and 4.89 MeV, respectively, for the proton $1f_{5/2}$, $2p_{1/2}$, and $1g_{9/2}$ orbitals (relative to the value of the $2p_{3/2}$ orbital). For neutron $1g_{7/2}$, $3s_{1/2}$, $2d_{3/2}$ orbitals, we used the single-particle energy values of 3.33, $-0.39$, and 1.73 MeV (relative to the value for the $2d_{5/2}$ orbital), respectively. These values have been chosen in the following way. Since the proton-proton interaction for the $1f_{5/2}$, $2p_{1/2}$, and $1g_{9/2}$ orbitals is the one empirically determined by Ji and Wildenthal [19] to describe many nuclei with $Z \geqslant 32$ and $N = 50$, the single-particle energies of proton orbitals used in our calculations were renormalized in such a way that by taking into account the additional proton-neutron interaction between the $1f_{5/2}$, $2p_{3/2}$, $2p_{1/2}$, and $1g_{9/2}$ protons and the $2p_{1/2}$ and $1g_{9/2}$ neutrons, the calculations still reproduce the results of Ji and Wildenthal, who did not consider the proton-neutron interaction explicitly. The neutron orbitals $2p_{1/2}$ and $1g_{9/2}$

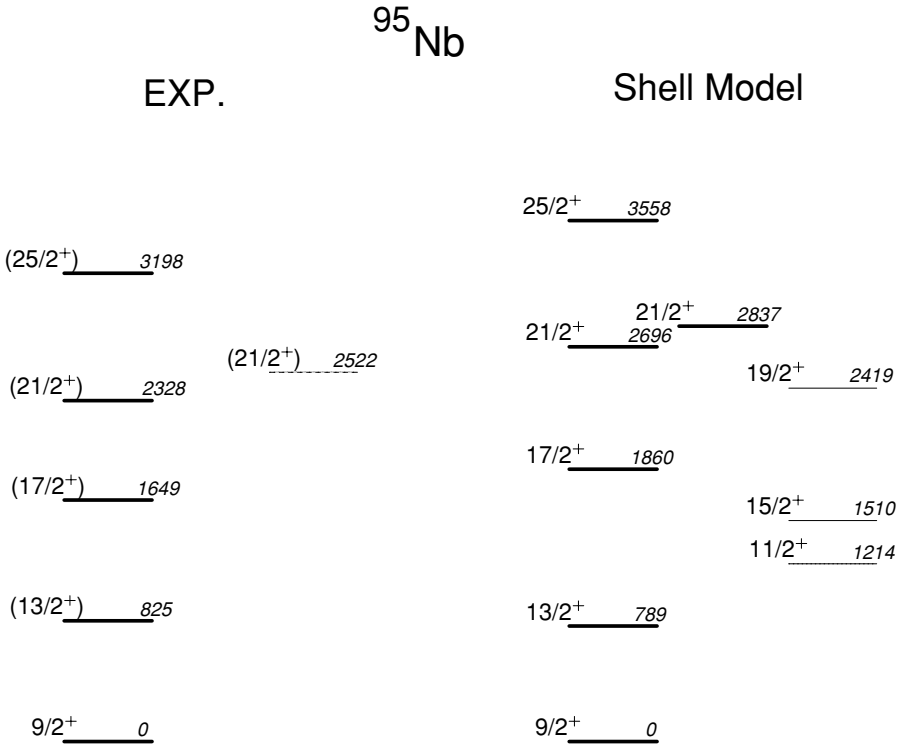


FIG. 9. Comparison of the experimental level scheme of $^{95}$Nb with shell-model calculations (see text for details).

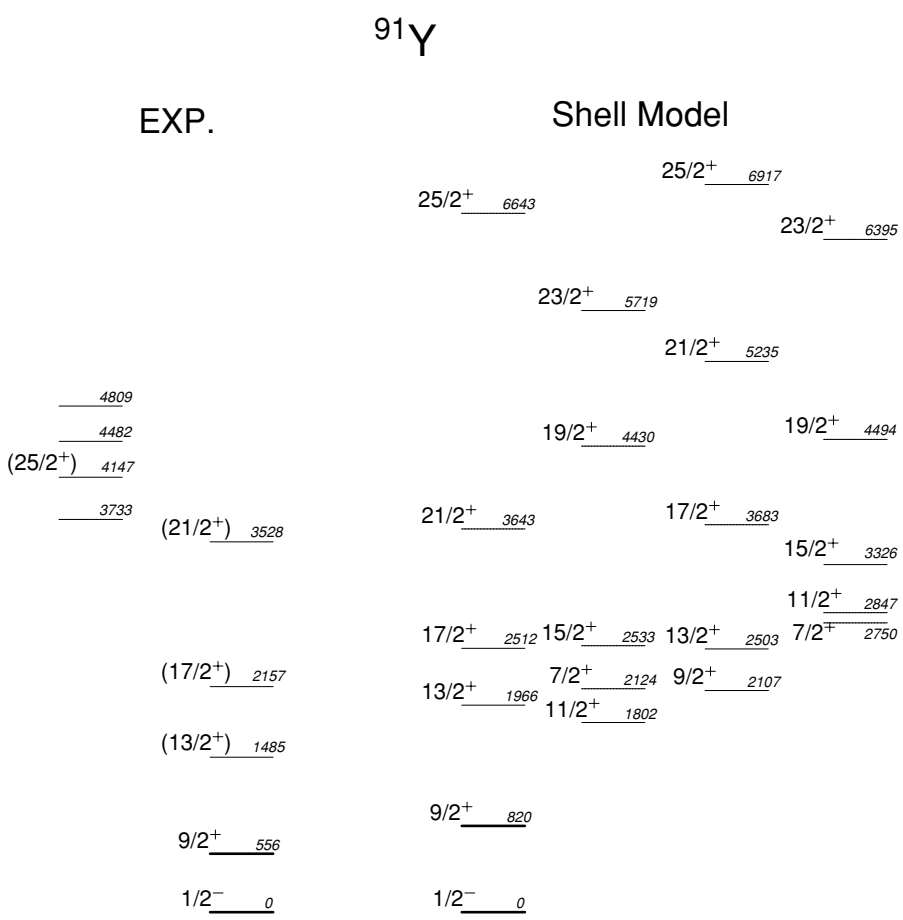


FIG. 10. Comparison of the experimental level scheme of $^{91}$Y with shell-model calculations (see text for details).

TABLE II. Occupation numbers of the spherical orbitals used in the present shell-model calculations for $^{95}$Nb and $^{91}$Y.

| | Protons | | | | Neutrons | | | |
|---|---|---|---|---|---|---|---|---|
| State | $1f_{5/2}$ | $2p_{3/2}$ | $2p_{1/2}$ | $1g_{9/2}$ | $1g_{7/2}$ | $2d_{5/2}$ | $2d_{3/2}$ | $3s_{1/2}$ |
| | | | | $^{95}$Nb | | | | |
| $9/2_1^+$ | 6 | 4 | 1.93 | 1.07 | 0.05 | 3.23 | 0.48 | 0.24 |
| $13/2_1^+$ | 6 | 4 | 1.95 | 1.05 | 0.04 | 3.36 | 0.35 | 0.25 |
| $17/2_1^+$ | 6 | 4 | 1.93 | 1.07 | 0.07 | 2.98 | 0.77 | 0.18 |
| $21/2_1^+$ | 6 | 4 | 1.91 | 1.09 | 0.52 | 2.75 | 0.59 | 0.14 |
| $21/2_2^+$ | 6 | 4 | 1.91 | 1.09 | 0.54 | 2.70 | 0.62 | 0.14 |
| $25/2_1^+$ | 6 | 4 | 1.90 | 1.11 | 1.00 | 2.52 | 0.26 | 0.22 |
| $29/2_1^+$ | 6 | 4 | 0.16 | 2.84 | 0.89 | 1.56 | 0.35 | 1.20 |
| $33/2_1^+$ | 6 | 4 | 0.00 | 3.00 | 1.02 | 1.44 | 0.12 | 1.42 |
| | | | | $^{91}$Y | | | | |
| $9/2_1^+$ | 5.77 | 3.58 | 0.55 | 1.10 | 0.02 | 1.58 | 0.09 | 0.31 |
| $13/2_1^+$ | 5.77 | 3.55 | 0.58 | 1.10 | 0.02 | 1.63 | 0.10 | 0.25 |
| $17/2_1^+$ | 5.73 | 3.57 | 0.60 | 1.10 | 0.03 | 1.75 | 0.20 | 0.02 |
| $17/2_2^+$ | 5.76 | 3.55 | 0.59 | 1.10 | 0.22 | 1.20 | 0.50 | 0.08 |
| $19/2_1^+$ | 5.82 | 3.23 | 0.89 | 1.06 | 0.49 | 1.36 | 0.14 | 0.01 |
| $19/2_2^+$ | 5.81 | 3.29 | 0.83 | 1.07 | 0.52 | 1.39 | 0.08 | 0.01 |
| $21/2_1^+$ | 5.76 | 3.56 | 0.56 | 1.12 | 1.00 | 0.99 | 0.01 | 0.00 |
| $21/2_2^+$ | 5.80 | 2.96 | 1.23 | 1.01 | 0.05 | 1.86 | 0.08 | 0.01 |
| $25/2_1^+$ | 5.54 | 3.28 | 1.16 | 1.02 | 1.00 | 1.00 | 0.00 | 0.00 |

were kept fully occupied, and hence they do not influence the wavefunctions and the level energies relative to the ground state. For the neutron $2d_{5/2}$, $1g_{7/2}$, $3s_{1/2}$, and $2d_{3/2}$ orbitals, the single-particle energy values were chosen to obtain a good description of the low-energy spectra in $^{93}$Mo, $^{91}$Zr, and $^{89}$Sr.

Figure 9 shows the comparison of the experimental spectrum of $^{95}$Nb with the results of these calculations. A reasonably good agreement has been obtained for yrast states with spin up to 25/2. The higher-spin states are predicted to lie much higher in energy than observed experimentally. Table II shows the particle occupation of the orbitals included in the calculations. It can be observed in Table II that the calculated states with spin above 25/2 require the excitation of one proton pair from the $2p_{1/2}$ to the $1g_{9/2}$ orbital, as well as the promotion of one neutron from the $2d_{5/2}$ to the $3s_{1/2}$ orbital. Clearly, an enlargement of our basis space by including the $1h_{11/2}$ intruder orbital and allowing the competition of many other configurations (particle-hole excitations across $Z = 38$ and $N = 50$) will increase the collectivity and lower the energy of these states, as required by the experiment.

To calculate the $^{91}$Y nucleus, we allowed at most two holes in the $1f_{5/2}$ and $2p_{3/2}$ proton orbitals. The comparison between the experimental level scheme and the predicted one is shown in Fig. 10, and selected wavefunctions are given in Table II. The positive-parity yrast states are well described up to spin parity $21/2^+$. For the experimental levels placed above this state (see Fig. 3), unambiguous spin-parity assignments were

not possible, and they cannot be precisely associated with calculated states. They most likely correspond to some of the $17/2^+$, $19/2^+$, or $21/2^+$ states predicted by our calculations in their energy region (see Fig. 10). Higher-spin levels are predicted at high energies. For example, the $25/2^+$ state is predicted above 6 MeV in our calculations since it can be built only by promoting at least one proton across the $Z = 38$ shell gap (from the $1f_{5/2}$ or $2p_{3/2}$ orbitals into the $2p_{1/2}$ orbital), as can be seen from the orbital occupancies given in Table II. As in the case of $^{95}$Nb, a shell-model space extended to include the neutron $1h_{11/2}$ orbital and a more relaxed truncation scheme should be considered for a good description of higher-spin states in $^{91}$Y.

## V. CONCLUSIONS

The positive-parity yrast states of the nuclei $^{91}$Y and $^{95}$Nb have been assigned in experiments utilizing heavy-ion fusion-evaporation reactions. Shell-model calculations have been performed for both nuclei with the OXBASH shell-model code using the configuration space ($\pi f_{5/2}, \pi p_{3/2}, \pi p_{1/2}, \pi g_{9/2}, \nu p_{1/2}, \nu g_{9/2}, \nu d_{5/2}, \nu g_{7/2}, \nu s_{1/2}, \nu d_{3/2}$). For $^{95}$Nb, an inert $^{88}$Sr core has been considered; while in the case of $^{91}$Y, up to two holes in the proton $f_{5/2}$ and $p_{3/2}$ orbitals were allowed. These calculations describe reasonably well the level schemes up to the $25/2^+$ state in $^{95}$Nb and the $21/2^+$ state in $^{91}$Y. To describe states of higher spin, an enlargement of the configuration space is needed.

## ACKNOWLEDGMENTS

We acknowledge support received within the European Contract No. HPRI-CT-1999-00083–V Framework Programme. This work was partially funded by EPSRC (UK).

[1] O. Horibe, Y. Mizumoto, M. Kawamura, J. Phys. Soc. Jap. **42**, 1803 (1977); J. K. Halbig, F. K. Wohn, W. L. Talbert, J. J. Eitter, J. R. McConnell, Nucl. Phys. **A203**, 532 (1973).
[2] B. M. Preedom, E. R. Flynn, and N. Stein, Phys. Rev. C **11**, 1691 (1975).
[3] B. M. Preedom, E. Newman, and J. C. Hiebert, Phys. Rev. C **166**, 1156 (1968); J. C. Hardy, W. G. Davies, and W. Darcey, Nucl. Phys. **A121**, 103 (1968).
[4] R. J. Peterson and H. Rudolph, Nucl. Phys. **A241**, 253 (1975).
[5] C. M. Baglin, Nucl. Data Sheets **86**, 1 (1999).
[6] M.-M. Be, B. Duchemin, E. Browne, S.-C. Wu, V. Chechev, R. Helmer, and E. Schonfeld, CEA-ISBN 2-7272-0211-3 (1999).
[7] K. P. Lieb *et al*., Phys. Rev. C **2**, 1822 (1970).
[8] M. S. Zisman *et al*., Phys. Rev. C **8**, 1866 (1973); L. R. Medsker and J. L. Yntema, *ibid*. **7**, 440 (1973); M. S. Zisman and B. G. Harvey, *ibid*. **5**, 1031 (1972); P. K. Bindal, D. H. Youngblood, and R. L. Kozub, *ibid*. **10**, 729 (1974).
[9] E. R. Flynn, R. E. Brown, F. Ajzenberg-Selove, and J. A. Cizewski, Phys. Rev. C **28**, 575 (1983).
[10] J. L. Schoonover *et al*., Nucl. Phys. **A234**, 331 (1974).
[11] T. W. Burrows, Nucl. Data Sheets **68**, 635 (1993).
[12] Zs. Podolyák *et al*., Int. J. Mod. Phys. E **13**, 123 (2004).
[13] D. Bazzacco, in Proceedings of the International Conference of Nuclear Structure at High Angular Momentum, Ottawa, 1992, Report No. AECL 10613, Vol. II, p. 376 (unpublished).
[14] C. M. Baglin, Nucl. Data Sheets **80**, 1 (1997).
[15] N. Fotiades *et al*., Phys. Rev. C **65**, 044303 (2002).
[16] B. Kharraja *et al*., Phys. Rev. C **57**, 2903 (1998).
[17] B. A. Brown, A. Etchegoyen, W. D. M. Rae, and N. S. Godwin, Computer Code OXBASH, MSU NSCL Report No. 524, 1984 (unpublished).
[18] A. Hosaka, K. I. Kubo, and H. Toki, Nucl. Phys. **A444**, 76 (1985).
[19] X. Ji and B. H. Wildenthal, Phys. Rev. C **37**, 1256 (1988).
[20] D. H. Gloeckner, Nucl. Phys. **A253**, 301 (1975).
[21] J. D. Serduke, R. D. Lawson, and D. H. Gloeckner, Nucl. Phys. **A256**, 45 (1976).